

Data diversity for UXO discrimination in realistic settings with a handheld EMI sensor

Kevin O'Neill⁽¹⁾, IJ Won⁽²⁾, Alex Oren,⁽²⁾ Chi-Chih Chen⁽³⁾, Hyoun-Sun Youn⁽³⁾, Xudong Chen⁽⁴⁾,
and Keli Sun⁽⁵⁾

⁽¹⁾ERDC - CRREL, 72 Lyme Rd, Hanover NH 03755, Kevin.ONeill@ERDC.usace.army.mil

⁽²⁾Geophex Ltd, 305 Mercury St, Raleigh NC

⁽³⁾The Ohio State University Electrosience Laboratory, Kinnear Rd, Columbus OH

⁽⁴⁾The Center for Electromagnetic Theory and Application, MIT, Mass Ave, Cambridge MA

⁽⁵⁾The Thayer School of Engineering, Dartmouth College, Hanover, NH 03755

ABSTRACT

Electromagnetic induction sensing (EMI), between ~ 10's of Hz and 100's of kHz, may show the strongest promise for discrimination of subsurface, shallow metallic objects such as unexploded ordnance (UXO). While EMI signals penetrate the soil readily, resolution is low and responses are sometimes ambiguous. For crucial discrimination progress, maximum data diversity is desirable in terms of look angles, frequency spectrum, and full vector scattered field data. Newly developed instrumentation now offers the possibility of full vector UWB EMI data with flexible look angle and sensor distance/sweep, defined by precise laser positioning. Particulars of the equipment and resulting data are displayed. An indication is given of potential advantages for reducing the chronic ill-conditioning of inversion calculations with EMI data, when one takes advantage of the data diversity made possible by the instrumental advances. Some EMI measurement issues cannot be solved by EMI data diversity, as when small surface clutter above a much larger UXO effectively blinds an EMI sensor. EMI surveying must be supplemented by or sometimes replaced by ground penetrating radar (GPR) approaches in such instances.

I. INTRODUCTION

Electromagnetic induction remote sensing (EMI, 10's of Hz up to ~ 100's of kHz) may offer the best hope for reliable discrimination of UXO. As attention has focused on it, suggestive studies have been performed and new instruments developed [1-11]. Unfortunately, omnipresent metallic clutter at UXO cleanup sites complicates matters because EMI devices are essentially metal detectors. Clutter contributes very substantially to the very high false alarm rate in surveying at such sites, where typically 75% of cleanup costs go to careful excavation of innocuous items or empty holes. Broadband EMI usually penetrates the soil without impediment or distortion, while responding to the particulars of object geometry and composition. At the same time, resolution is very low, and many objects produce similar response spectra.

Consider the basic setup illustrated schematically in Figure 1. In an EMI antenna in which the transmitters and receivers are typically wire loops, the transmitted "primary" magnetic field fans out from a horizontal loop,

impinging upon a metallic object. Like the transmitter, this target becomes something of a magnetic dipole, producing its own secondary fan of magnetic field lines. Reception and recording of these secondary fields produces the received signal. Particularly because the magnetic dipole induced in an elongated object tends to orient itself towards the greatest dimension or axis of the scatterer, at the antenna position the secondary field may contain significant horizontal field components (see Figure). Normally, in frequency domain systems to date, only the vertical scattered field component has been measured.

II. THE GEM-3D

To assist in achieving data diversity sufficient to form more unambiguous UXO vs clutter signatures, Geophex Ltd has designed and constructed the GEM-3D sensor (Figure 2), based on its established GEM-3 device [2]. Like the GEM-3, the GEM-3D contains "horizontal" transmitter coils, which can actually easily be oriented in any direction. The sensor is handheld via a bar of negotiable length. Around the central cavity is a horizontal receiver coil, where the counterbalanced transmitting coils nullify the primary field so that the secondary field may be apprehended. Two vertical receiving coils, i.e. with horizontal axes, were emplaced around this same cavity. Little of the primary field should register in these new vertical receivers. This is partly because of the primary field nullification around the middle of the sensor head. Beyond that, the vertical coils cut through the azimuthally symmetrical fan of primary field lines in such a way that, for perfect geometry, those field lines are all tangential to the planes of the new coils. Thus there is no primary magnetic field flux through the vertical coils. Any flux recorded by them should be from the secondary field, which we seek. Because the physical structure of the antenna is rigid, any small residual primary field flux through the vertical coils can be calibrated out.

The measured data displayed in Figure 3 attest to the success of this design. Interestingly, the secondary H_x and H_y components change sign when they impinge on the vertical coils from one side vs the other. This adds particularly unambiguous indication of the target location, where these horizontal components pass through zero. The clear anti-symmetry of these components in the top row also underscores the fact that the UXO is vertically oriented, otherwise either the H_x or the H_y components would not be symmetrical in magnitude about the center line. When the UXO is horizontal, the secondary field distributions also reflect that fact, in the bottom row of plots. Here, because the UXO itself varies in material and geometry from one end to the other, we note the slight lack of magnitude symmetry in the H_x component, but not in H_y . In the least, all three components appear clearly, without distortion caused by "leakage" of the primary field. Detailed validation of the field magnitudes in GEM-3D data is provided by comparison to analytical solutions of EMI scattering from canonical shapes, compared to data [12,13].

III. LASER POSITIONING

The data collected in Figure 3 were obtained by manually moving the antenna over a measurement grid, i.e. a template of positions above the scatterer. This is a time consuming, tedious, and error-producing process. Ideally, we would like to move the antenna freely while retaining the kind of information in Figure 3, even if the sensor head is tilted. Note that when it is tilted one still obtains complete definition of the vector scattered field, while illuminating the target from different angles. In general, oblique look angles may be desirable for some target configurations. For the geometries in Figure 1 and Figure 2, oblique illumination of the target location is only obtained indirectly, because of the spreading of the field lines from the horizontal transmitter loops. This provides relatively weak oblique illumination. In any case, such free movement in tilted orientations may be required by uneven terrain, e.g. embankments. Combined theoretical and measurement studies also suggest that there may be discrimination benefits to be had by systematically varying the antenna elevation, particularly in cluttered environments. We pursue this a little below.

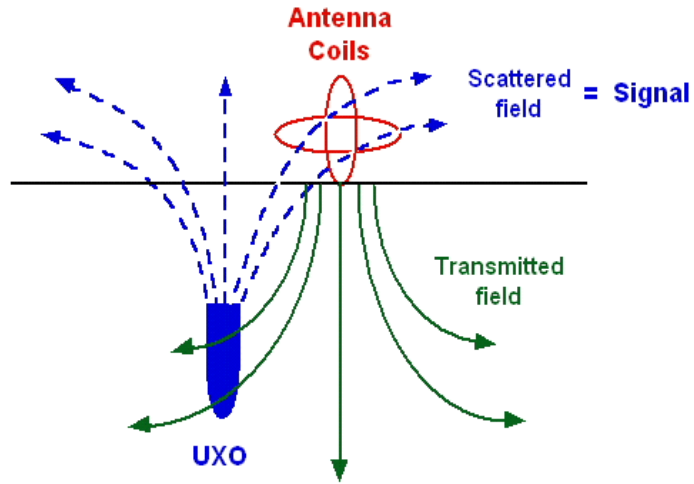


Figure 1. EMI antenna transmitting a primary magnetic field and receiving as scattered signal, the secondary magnetic field produced by the target.



Figure 2. The GEM-3D, indicating one horizontal and two vertical receiving coils. Like the horizontal receiving coil, the two horizontal transmitting coils are encased in the disk.

Examination of all magnetic field components, from different views of the target, shows details of symmetry, asymmetry, and a distribution of signal reflecting the UXO's shape

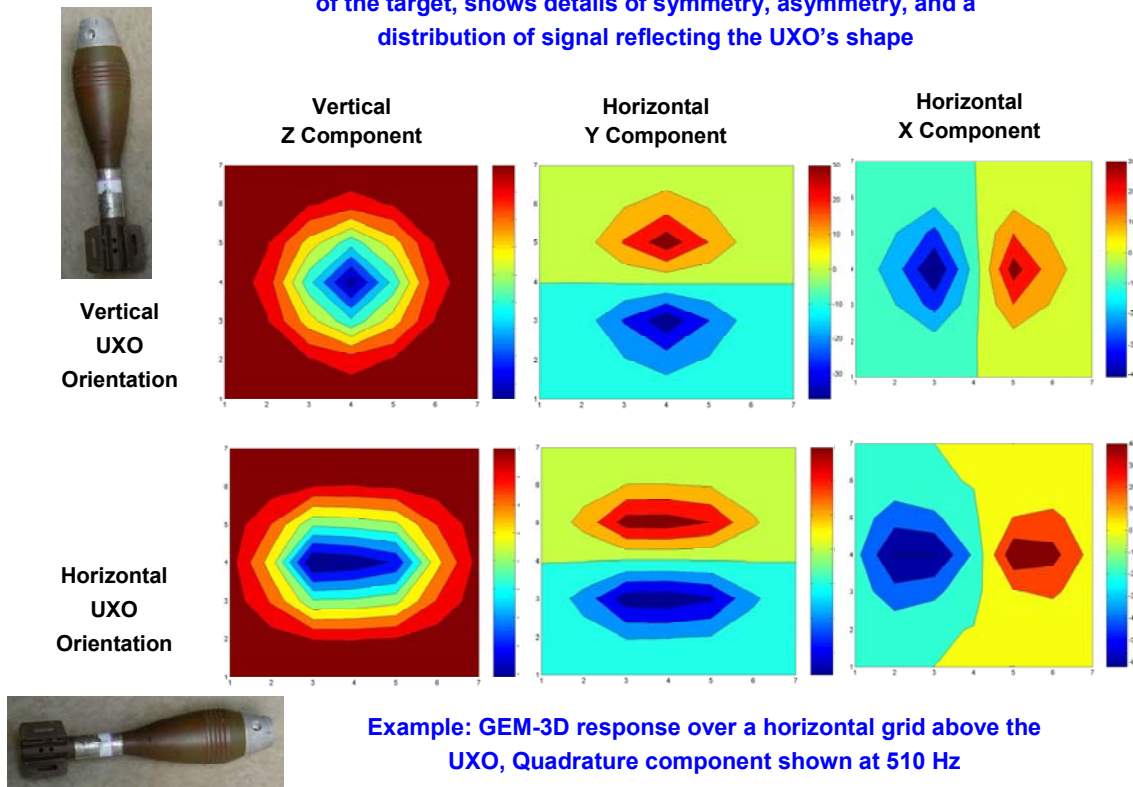


Figure 3. GEM-3D measurements over a plane above a UXO in vertical orientation (top row) and horizontal orientation (bottom row), where the Z axis is perpendicular to the plane of the sensor head. Left plots: scattered Z field component; middle, H_y component; right, H_x component, i.e. in direction aligned with the axis of the UXO when it is horizontal.

To achieve the desired positioning, we have integrated an Arcsecond laser positioning system into the GEM-3D sensor (Figure 4). The laser system features two or more eye-safe spinning laser transmitters, which are placed at reference positions somewhere near the terrain of interest. The distance between laser transmitters and receivers is partly a function of the power of the particular system being used, the number of transmitters, and the needs of the survey. With standoff on the orders of ~ 10 of meters, positional accuracy on the order of less than 1 mm is achievable. The known locations of the transmitters, angles of transmissions, and timing of laser signals allows determination of the positions of three receivers attached to the EMI sensor. That in turn allows precise inference of both X,Y,Z position of the center of the sensor head as well as all tilt angles. Using more transmitters can alleviate limitations caused the line-of-sight nature of the system. The sensor head on the right in the figure has been blackened to minimize unwanted laser reflections, and the tubular structures are amplifiers of the laser receiver signals. To minimize interference between the EMI and laser systems, both laser receivers and amplifiers can be moved off the sensor head and onto a frame rigidly attached some distance up the handle attached to it. In the configuration shown in the figure, this combined EMI and laser positioning system has successfully produced both induction and position data such that that information can be recorded together in common formats, eliminating any co-registration issues.

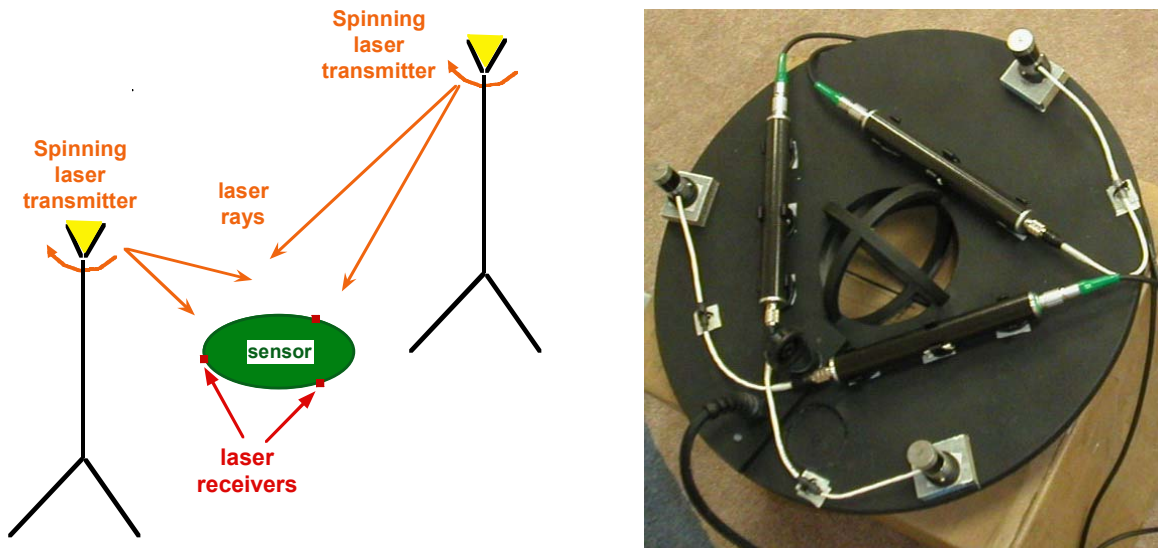


Figure 4. Addition of laser positioning system to the GEM-3D.

IV. BENEFITS OF EMI DATA DIVERSITY

It could be argued that much of the information provided by the horizontal received components in Figure 3 is redundant, relative to reception of the vertical (H_z) component alone. Depending on the model of UXO EMI response one employs, in principle one might be able to infer target parameters from the more restricted data alone. However here is where theoretical appearance and practical reality diverge. Like most inversion calculation, inference of EMI target parameters from measured signals over a restricted grid or plane is often plagued by ill-conditioning. Further, we have recently defined a complete target signature modeling system, the Standardized Excitation Approach (SEA). The SEA models include all relevant scattering effects, with negligible idealization, including heterogeneous composition, non-uniform illumination, internal interactions within the target, near and far field effects. Complete signature models such these have been shown to be necessary, at least under certain circumstances, to reflect basic signal behaviors for realistic targets. The signature system works by decomposing any arbitrary primary field into basic components, either mathematical eigenfunctions or fields transmitted by some standardized set of hypothetical equivalent sources. Then the response of the target to each of these basic stimuli is inferred. The scattering parameters defining each of these basic responses are characteristics of the object investigated. Once they have been inferred in the course of general inversion, they can be examined for target classification. Alternatively, if inferred under controlled circumstances, they provide a forward scattering model for particular targets that is fast enough for use in either general inversion calculations or, in the least pattern, matching type classification algorithms [e.g. 14].

Pursuing this, we perform a simulation test using the spheroidal eigenfunction based SEA. Here we assume the existence of an object with two sections, one steel about 1 m long and another non-magnetic material about 30 cm long. This is placed at an arbitrary angle beneath the lowest of two measurement surfaces (surface #1), with the object spanning a depth of about 1 to 2 m. "Measurements" are provided at nine points on each grid by an analytical solution forward model for spheroids [13]. As noted in the caption of Figure 5, different combinations of field components and grid levels are exploited for data diversity in the construction of the matrices. The figure

shows results in terms of the condition number of the resulting matrices generated for the inversion problem, as we seek to infer the SEA scattering coefficients. That is, we have divided the condition number (ratio of largest to smallest matrix eigenvalue) of each matrix by that of the matrix for the maximum information case #1, i.e. with all three vector components measured over two levels. We note that the same measurements performed only over surface #1 produce a condition number some four orders of magnitude worse. Interesting, measuring a single component over the two levels does not produce much worse results than measuring all components over only a single level. Measuring only the single H_z component over only a single level, today's norm, produces the worst condition number by many orders of magnitude. Doubtless, the details of this rather artificial test will be altered by the particulars of any real circumstance. Further, the absolute value of the condition number in some approaches may be sufficient, although it is not as good as that for the maximum information approach. Nevertheless, given that ill-conditioning is a pervasive and a severe problem, the observations incorporated in Figure 5 evidently point the way towards more secure inversion computations.

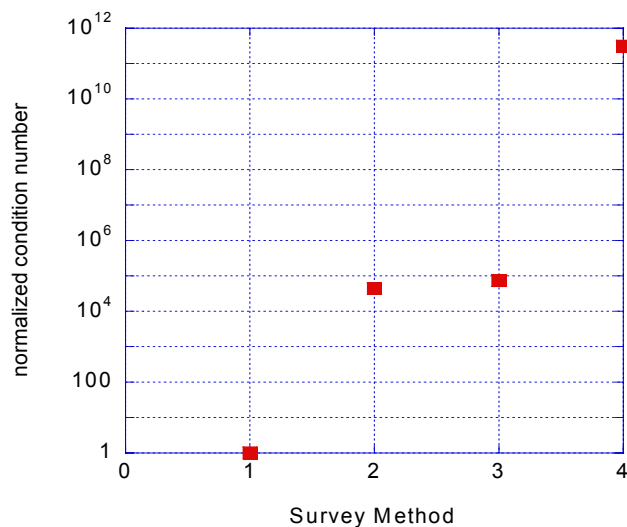


Figure 5. Ratio of condition number of the inversion system to that for the maximum data case, Method 1 using H_x , H_y , and H_z over two grid levels. Method 2 uses H_x , H_y , and H_z over surface #1 only; Method 3 uses H_z only over grids at 2 elevations; Method 4 uses H_z only over surface #1.

V. DIVERSITY BY SUPPLEMENTING EMI WITH GPR

Problems arise in EMI surveying of cluttered sites that cannot be cured by greater EMI data diversity. While we have shown elsewhere (e.g. Shamatava et al, these proceedings) that ground penetrating radar (GPR) data might be used to constrain EMI processing to considerable advantage, in some instances the conditions defeat EMI sensors to the point where no beneficial GPR assistance is possible. Below we pursue such an instance. In this case the discrimination survey can be beneficially supplemented by GPR in that GPR can function effectively under circumstances where EMI cannot perform at all.

Consider the setup shown in Figure 6, left, which shows a shallow layer of small clutter fragments above a much larger UXO. The distance from the sensor to the clutter layer remains fixed in this example; therefore the magnitude of the clutter signal S_c is also fixed at some value A_{co} . By contrast, idealizing the UXO as a dipole responder, we assume that the UXO signal S_u follows the common $1/R^6$ rule.

That is, S_u changes as $A_{u0} (R_{u0}/R_u)^6$, where R_u is the current UXO depth under consideration, R_{u0} is the initial i.e. shallowest depth considered (0.2 m), and A_{u0} is the UXO signal magnitude when the target is at 0.2 m. So, overall, one may examine cases with various possible "best" clutter to signal ratios A_{c0} / A_{u0} when the UXO signal is strongest (i.e. the target is at the shallowest depth considered) and then trace the change in relative signal strengths as deeper UXO positions are considered and the clutter signal remains fixed. We define a measure of visibility V of the UXO as $\log(S_u/S_c)$. When $V \sim 0$, the signal strengths of the two scatterers are about equal; $V > 0$ or $V < 0$ indicates orders of magnitude greater or lesser visibility, respectively. Figure 6, right, shows a contour plot of the fairly dismal implications of this simple model. The heavy line indicates the approximate boundary between visibility and invisibility, the region above the line being the zone of obscuration. For example, consider cases in which for, $A_{c0} / A_{u0} = 10^{-6}$, corresponding to the left edge of the contour plot. "Initially," i.e. at the bottom left corner of the plot, the UXO is very visible as $S_u/S_c \sim 10^6$. However one need only increase the depth considered for the UXO to values greater than about 0.5 m for its advantage to fade, and thereafter it quickly declines by orders of magnitude into obscurity. Towards the other side of the plot, if the relative clutter magnitude is about 10^{-2} for the initial UXO depth $R_{u0} = 0.2$ m, merely increasing the UXO depth much past 0.3 m pushes its signal into obscurity.

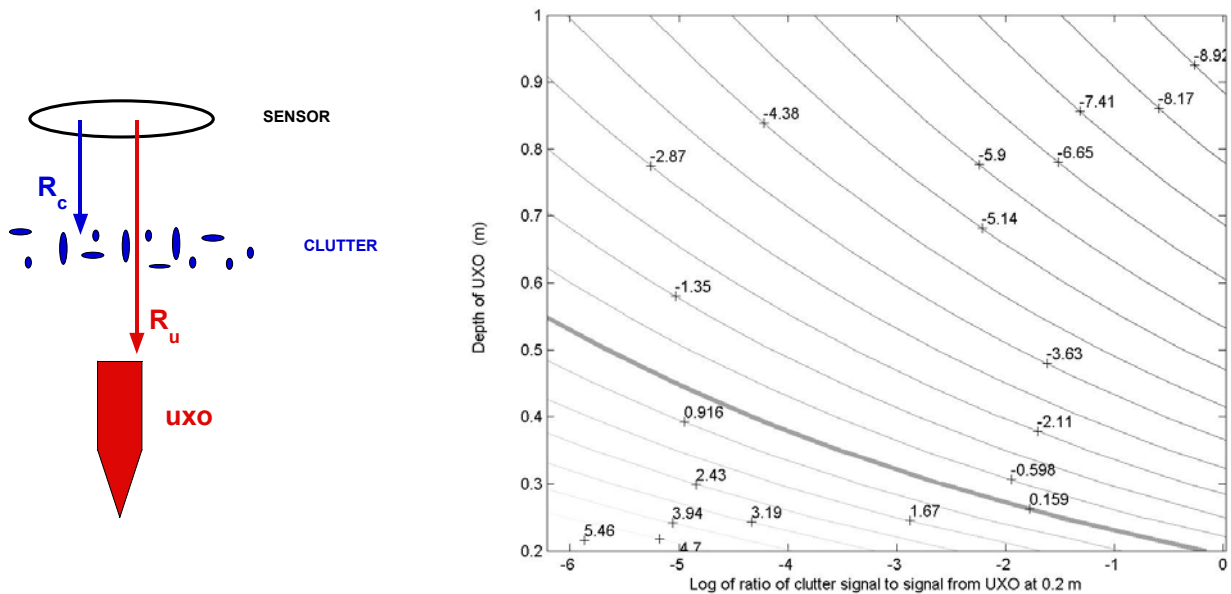


Figure 6. Left: Clutter layer above a UXO and below an EMI sensor. Right: Contours of Visibility of the UXO: Effect of UXO depth on its signal magnitude relative to clutter at a fixed shallower depth.

The observations above correspond to the reality we see in our measurements, in which widespread, small, shallow clutter items virtually blind the EMI sensor as we look for a much heftier UXO below. This was the case for the clutter shown in Figure 7 when a 105 mm projectile was buried about 30 cm below it, i.e. at 30 cm depth to the projectile's shallowest point, when the UXO axis was tilted downward at an angle of 45° . In contrast to the EMI experience, note the GPR profiles shown in Figure 8. The GPR scan was performed so that the antenna passed directly over the UXO, moving parallel to the target's axis, and the S_{11} component response is shown in the figure (both transmitted and received polarizations parallel to the scan direction). When there is no clutter present (top profile), one sees two relatively linear features near the left of the figure, rising from an arrival time (delay) of

about 25 ns, peaking at the UXO position and fading into typical hyperbolas as the antenna moves to the right, away from the target. The upper such curve is the earliest reflection from the upper end of the UXO, while the lower curve is from the bottom tip of the target. Evidence of the UXO is clear (to those accustomed to looking at such profiles). The middle profile shows results from the same scan but with surface clutter present. The impact of the clutter is negligible as far as visibility of the UXO is concerned. This is especially the case after frequency filtering (bottom plot) based on estimated resonance of the UXO, as would be performed in actual processing procedures. This is not to understate the difficulties that may affect GPR surveying of this sort. For example, note the plentiful signal clutter in the portions of the profiles above the UXO position. This is presumably due to simple ground disturbance of the rather homogeneous soil as the UXO was emplaced - not a very impressive environmental heterogeneity. The kind of metallic clutter in Figure 7 can obscure the UXO EMI signal altogether, under unfavorable circumstances. However here the clutter signal from the dispersed items is merely lost in that from surface and near-surface disturbance. For all practical purposes, the GPR sees right through the clutter screen.

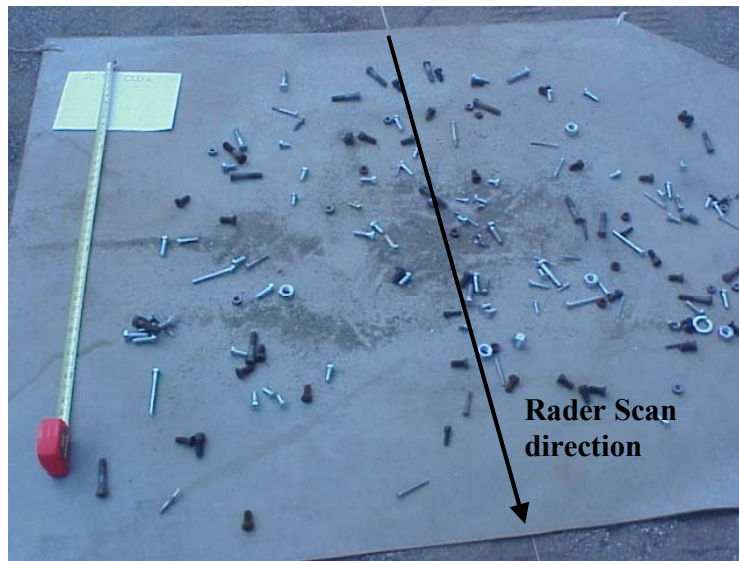


Figure 7. Distribution of small clutter items used at subsurface UXO sensing site.

VI. CONCLUSION

The benefits of electromagnetic induction sensing may be enhanced by introducing a new generation of data diversity into the processing. This is made possible by the development of a new UWB fully vector EMI handheld sensor. The handheld nature of the device allows for completely flexible deployment, which is only useful for advanced processing when combined with precise positioning data. That data are provided by the integration of a laser positioning system that tracks all X,Y,Z positions and tilt angles during arbitrary sensor motion. Numerical experiments suggest that this level of data definition and diversity can substantially benefit newly developed advanced signature modeling systems. While EMI signals penetrate the soil readily, induction sensors can be "blinded" by commonly occurring layers of dispersed, small metal fragments at UXO cleanup sites. Such an EMI measurement issue cannot always be solved by EMI data diversity alone. Induction sensing may be supplemented by or sometimes replaced by ground penetrating radar (GPR) approaches in such instances. Measurement exercises with small clutter above a substantial buried UXO show instances in which GPR can see right through shallow clutter layers that defeat EMI.

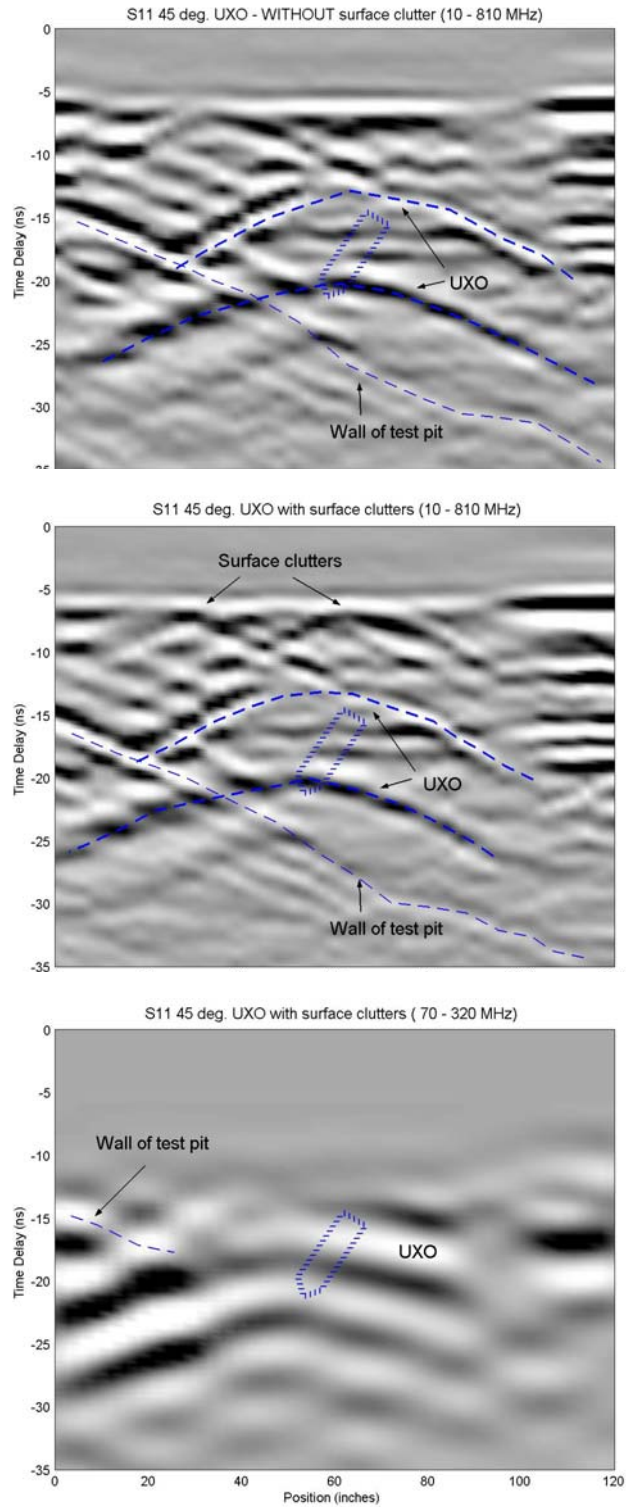


Figure 8. GPR profile from a scan over the UXO, in which the vertical axis is the signal arrival time and the horizontal axis is antenna position. Top: without surface clutter; Middle: with the surface clutter in Figure 7; Bottom: Cluttered case again, filtered, based on estimated UXO resonant frequency.

ACKNOWLEDGMENT: This work was sponsored in part by the Strategic Environmental Research and Development Program and US Army CoE ERDC BT25 and AF25 programs.

REFERENCES

1. J. M. Stanley and S.M. Griffin, Sub-Audio Magnetics - Simultaneous magnetic and electromagnetic detection of UXO, Proc. UXO/Countermining Forum, Orlando, Sept 3-6, 2002.
2. I.J.Won, D. A. Keiswetter, D. R. Hanson, E. Novikova, and T. M. Hall, GEM-3: A monostatic broadband electromagnetic induction sensor, J. Environ. Eng. Geophys., vol. 2, pp. 53–64, Mar. 1997.
3. T.H. Bell, B.J. Barrow, and J.T. Miller, Subsurface discrimination using electromagnetic induction sensors," IEEE Trans. Geosci. Remote Sensing, vol 39, No. 6, pp1286-1293, 2001.
4. D. A. Keiswetter, I.J. Won, B. Barrow, T. Bell, Object identification using multi-frequency EMI data, proc. UXO forum, 25-27 May 1999, Atlanta GA.
5. L. Collins, P. Gao, N. Geng, L. Carin, D. Keiswetter, and I. J. Won, Discrimination of UXO-like metal targets using wideband electromagnetic induction, proc. UXO forum, 25-27 May 1999, Atlanta GA.
6. L. Collins, P. Gao, and S. Tantum, J. Moulton, L. Makowsky, D. Reidy, and D. Weaver, A comparison of statistical signal processing algorithms for detection and identification of low metal mines, UXO Forum, Anaheim, 2-4 May 2000.
7. P. Gao, L. Collins, P.M. Garber, N. Geng, L. Carin. Classification of landmine-like metal targets using wideband electromagnetic induction, IEEE Trans. Geosci. Remote Sensing, Vol. 38, pp 1352-1361, 2000.
8. S.C. MacInnes, J. Durham, J. Dickerson, D.D. Snyder, and K.L. Zonge, Fast TEM for UXO mapping at Gambell, Saint Lawrence Island, Alaska, Proc. UXO/Countermining Forum, 9-12 April 2001, New Orleans, LA.
9. N.R. Carlson, and K. L. Zonge, Early-time, multi-component mobile TEM for deep metal detection, Proc. SAGEEP 2002, Las Vegas, NV: Environ. & Eng. Geophys. Soc.
10. S. C. MacInnes, D. D. Snyder, and K. L. Zonge, Physics-based characterization of UXO from multi-component TEM data, Proc. UXO/Countermining Forum, Orlando, FL, 3- 6 Sept 2002.
11. D. D. Snyder, D. C. George, S. C. MacInnes, and K. L. Zonge, Demonstration of a fast 4D TEM system at the NRL Baseline Ordnance Test Site, Proc. UXO/Countermining Forum, 3- 6 Sept 2002, Orlando, FL.
12. C.O Ao, H. Braunsch, K. O'Neill, and J.A. Kong, Quasi-magnetostatic solution for a conducting and permeable spheroid with arbitrary excitation, IEEE-Trans. Geosci. Remote Sensing, Vol 40, no 4, pp.887-897, 2002.
13. B. E. Barrowes, K. O'Neill, T. M. Grzegorzczuk, X. Chen and J. A. Kong, Broadband electromagnetic induction solution for a conducting and permeable spheroid, submitted for publ., 2003
14. X. Chen, K. O'Neill, B. E. Barrowes, T. M. Grzegorzczuk, and J. A. Kong, Application of a spheroidal mode approach with Differential Evolution in inversion of magneto-quasistatic data for UXO discrimination, submitted for publ, J. Inverse Probl.